Journal of Power Sources 266 (2014) 440–447

Contents lists available at ScienceDirect

Journal of Power Sources

journal homepage: www.elsevier.com/locate/jpowsour

High-efficiency dye-sensitized solar cells based on ultra-long single crystalline titanium dioxide nanowires

Lanfang Que, Zhang Lan*, Wanxia Wu, Jihuai Wu*, Jianming Lin, Miaoliang Huang

Engineering Research Center of Environment-Friendly Functional Materials, Ministry of Education, Key Laboratory of Functional Materials for Fujian Higher Education, Institute of Materials Physical Chemistry, Huaqiao University, Xiamen 361021, China

HIGHLIGHTS

- 3D networks of single crystalline TiO_2 nanowire membranes were grown on Ti foils.
- Self-standing TiO_2 nanowire membranes were used to fabricate front-side photoanodes.
- The highest power conversion efficiency of DSCs could attain to 8.05%.

ARTICLE INFO

Article history:
Received 17 March 2014
Received in revised form
22 April 2014
Accepted 6 May 2014
Available online 21 May 2014

Keywords:
Titanium dioxide nanowire membrane
Front-side illuminated photoanode
Photovoltaic performance
Dye-sensitized solar cell

ABSTRACT

High-efficiency dye-sensitized solar cells (DSCs) based on 3D networks of ultra-long single crystalline TiO_2 nanowires are fabricated. By hydrothermal reaction of Ti foils in alkali aqueous solution, following ion exchange and high temperature sintering processes, the ultra-long single crystalline TiO_2 nanowires can be prepared. Due to long enough of the TiO_2 nanowires, they not only form 1D arrays perpendicular to Ti foils, but also extend to form 3D network structure on the top-side of the arrays. By optimizing the hydrothermal duration at 24 h, the formed TiO_2 nanowire membrane based front-side illuminated photoanode shows enhanced dye-loading and light scattering abilities and excellent charge transport properties. So the DSC with this photoanode can attain to the highest power conversion efficiency about 8.05%.

1. Introduction

Dye-sensitized solar cells (DSCs) have received considerable interest as one of the most promising alternatives for cost-intensive silicon-based photovoltaic devices due to its advantages of clean materials, competitive prices, and an easy, eco-friendly fabrication process [1]. Central to a DSC is the photoanode which supplies large surface area to adsorb sufficient dye molecules to harvest sun light and provides pathways for electron transportation, moreover, it is even required to provide high light scattering ability for enhancing absorption of red and near-infrared light [2]. In order to obtain large surface area in the photoanode, 10–20 nm TiO_2 nanoparticles are usually used to construct 8–12 μm thick mesoporous film [3]. However, it is found that the transportation of photogenerated electrons in the TiO_2 nanoparticle mesoporous film proceeds by a trap-limited diffusion process [4,5]. And the photogenerated electrons need to diffuse through 10^3–10^6 nanoparticles to reach the conductive substrate [6]. So considerable number of photogenerated electrons may be recombined by the dark reaction when they diffuse in the film. This disadvantage limits the thickness of TiO_2 nanoparticle mesoporous film to adsorb more dye molecules to further increase the power conversion efficiency of the DSC, which also results in the negligible light scattering ability of the film to utilize the red and near-infrared light.

Compared to the disordered TiO_2 nanoparticle mesoporous film, the oriented one-dimensional (1D) arrays such as nanowires, nanotubes and nanorods are expected to greatly promote electron transport by providing a direct conduction pathway for rapid collection of photogenerated electrons, which can also diminish the charge recombination obviously [7,8,21]. However, despite the advantages, the power conversion efficiency of such DSCs based on oriented 1D TiO_2 nanowire arrays still remain lower value than that (12%) of DSCs made of TiO_2 nanoparticle mesoporous film [1,9]. The primary reason is owing to the much lower internal surface area of

* Corresponding authors. Tel.: +86 595 22690582; fax: +86 595 22693999.
E-mail addresses: lanzhang@hqu.edu.cn (Z. Lan), jhwu@hqu.edu.cn (J. Wu).

http://dx.doi.org/10.1016/j.jpowsour.2014.05.022
0378-7753/

the 1D TiO_2 nanowire arrays film compared to TiO_2 nanoparticle mesoporous film, which leads to insufficient dye adsorption, and therefore low light harvesting efficiency. In order to increase the internal surface area, the oriented hierarchical TiO_2 nanowire arrays were prepared by Kuang et al. [10,11]. The power conversion efficiency of DSCs based on such structured photoanodes shows a significant enhancement compared to the original smooth ones. Another feasible way to enhance dye adsorption then finally enhance the power conversion efficiency of DSCs is to increase the length of nanowire arrays. The typical example is done by Gao et al., who synthesize multilayer assemblies of ZnO nanowire arrays for DSCs [12]. It is found that the internal surface area of the four layer assembly (about 40 μm) is five times larger than what can possibly be obtained with a single layer array (about 10 μm), and the power conversion efficiency of the DSC based on the four layer assembly is 7%, which is much higher than that of the DSC based on the single layer array (2.1%). Kuang et al. reported a classical method to prepare ultra-long anatase TiO_2 nanowire arrays with multi-layered configuration on fluorine doped tin oxide over-layer conductive glass (FTO glass) for high-efficiency dye-sensitized solar cells [13]. The length of multi-layered anatase TiO_2 nanowire arrays can be tuned in the range of 15–55 μm. The power conversion efficiency of the DSC based on 47 μm TiO_2 nanowire arrays can attain to the highest value of 9.40%.

Here, we try to fabricate high-efficiency DSCs based on 3D networks of ultra-long single crystalline TiO_2 nanowires. The ultra-long single crystalline TiO_2 nanowires can be prepared by hydrothermal of Ti foils in alkali aqueous solution [14]. Due to long enough of the TiO_2 nanowires, they not only form 1D arrays perpendicular to Ti foils, but also extend to form 3D network structure on the top-side of the arrays. The special morphology can increase dye adsorption and light scattering efficiency. Moreover, the ultra-long single crystalline TiO_2 nanowires can form excellent electron transport channels. Taking into accounts of these benefits, it can be expected to fabricate high-efficiency DSCs.

2. Experimental

2.1. Materials

Sodium hydroxide, titanium tetrachloride, hydrochloric acid, sodium iodide, tetrabutyl ammonium iodide, 4-*tert*-butylpyridine, iodine, acetonitrile, acetone, 2-propanol, ethylene glycol, ammonium fluoride, and ethanol were all A. R. Grade and purchased from Sinopharm Chemical Reagent Co., Ltd, China. The reagents were used without further treatment. Ti-foils (99%, purchased from Baoji Yunjie Metal Production Co., Ltd) were used as raw materials to synthesize TiO_2 nanowires. FTO glasses were purchased from Nippon Sheet Glass Co., JP (15 $\Omega\ \square^{-1}$). Sensitizing dye *cis*-$[(dcbH_2)_2Ru(SCN)_2]^{2-}$, $2(n\text{-}C_4H_9)_4N^+$ ($dcbH_2$ = 2, 2′-bipyridine-4, 4′-dicarboxylic acid) (N719) was purchased from Dye sol.

2.2. Preparation of self-standing TiO_2 nanowire membranes

TiO_2 nanowire membranes were synthesized on Ti-foil by a three-step synthesis method. Firstly, the Ti-foil was degreased by ultrasonic processing in acetone, 2-propanol, and ethanol for 15 min, respectively. Then it was put into 40 mL 1 M NaOH aqueous solution in a 80 mL Teflon-lined stainless steel autoclave. The autoclave was kept in an electric oven at 220 °C for 24 h. After cooling down to room temperature, the sample was washed with deionized water 5 times and dried in room temperature. Secondly, the sample was immersed in 0.5 M HCl aqueous solution for 2.5 h in order to exchange Na^+ ions with H^+ ions. At last, the as-prepared sample was calcinated at 450 °C for 30 min. The samples were also prepared by varying hydrothermal duration from 16 to 32 h.

Free-standing TiO_2 nanowire membranes were obtained by separating them from Ti foils with anodization and chemical etching methods [15,16]. The detailed processes are that the Ti foils with sintered TiO_2 nanowire membranes were anodized in the electrolyte containing ethylene glycol, H_2O (0.5 vol.% vs ethylene glycol), and ammonium fluoride (0.25 wt.% vs ethylene glycol) at 60 V for 5 min, and then immersed into H_2O_2 30 wt.% aqueous solution for 1 h to detach the TiO_2 nanowire membranes.

2.3. Preparation of dye-sensitized solar cells with TiO_2 nanowire membranes based photoanodes

Firstly, the front-side illuminated TiO_2 nanowire membranes based photoanodes were prepared. FTO glasses with size of 2.0 cm × 1.5 cm were ultrasonic vibrated in acetone and isopropanol to wash away any impurities. A blocking layer about 350 nm on the FTO glass was prepared by spin-casting two times of the TiO_2 quantum dots toluene solution at a rate of 4000 rpm for 1 min, and then sintered at 450 °C for 30 min [17]. A paste containing TiO_2 nanocrystalline particles with size about 10–20 nm was used as cementing agent to cohere the free-standing TiO_2 nanowire membranes on the FTO glasses with blocking layers. The thickness of the bonding layer is about 2.5–3 μm. After sintered at 450 °C for 30 min, the photoanodes were immersed in 0.05 M aqueous solution of $TiCl_4$ at 70 °C for 30 min, and then sintered again on the same condition. Finally, the photoanodes were sensitized with 2.5×10^{-4} M absolute ethanol solution of N719 at room temperature for 24 h.

Secondly, a photoanode and a platinum counter electrode were clipped together. One drop of liquid electrolyte was kept between the two electrodes. A piece of cyanoacrylate adhesive (30 μm) was used as sealant. Bisphenol A epoxy resin was used for further sealing process. The liquid electrolyte contained 0.4 M sodium iodide, 0.1 M tetrabutyl ammonium iodide, 0.5 M 4-*tert*-butylpyridine, and 0.05 M iodine in acetonitrile solution. There were five different photoanodes prepared in this work. The DSCs based on TiO_2 nanowire membranes prepared with different hydrothermal duration (as 16 h, 20 h, 24 h, 28 h, 32 h) are labeled as DSC-16, DSC-20, DSC-24, DSC-28 and DSC-32, respectively.

2.4. Measurements

The morphologies of TiO_2 nanowire arrays were observed by a field emission transmission electron microscopy (FETEM) (JEM-2100) and a field emission scanning electron microscopy (FESEM) (S-4800, HITACHI), respectively. X-ray Diffraction (XRD) measurements were performed with a Bruker D8 Advance X-ray diffractometer using Cu Kα radiation (λ = 1.5418 Å). UV–Vis absorption and diffused reflection spectra were measured by a Lambda 950 UV/Vis-NIR spectrophotometer. Intensity-modulated photovoltage spectroscopy (IMVS) and intensity-modulated photocurrent spectroscopy (IMPS) measurements were carried out on a CIMPS-4 system (Zahner, Zennium) with a frequency response analyzer under a modulated green light emitting diodes (530 nm) driven by a source supply (Zahner, PP211), which can provide both dc and ac components of the illumination. The modulated light intensity was 10% or less than the base light intensity. The frequency range was set from 10 kHz to 0.1 Hz. Electrochemical impedance spectroscopy (EIS) data were recorded using a CHI 660E electrochemical workstation with the frequency range from 0.01 Hz to 100 kHz. The magnitude of the alternative signal was 5 mV. The impedance measurements were carried out under forward bias of −0.8 V in the dark condition. The impedance spectra were analyzed with the

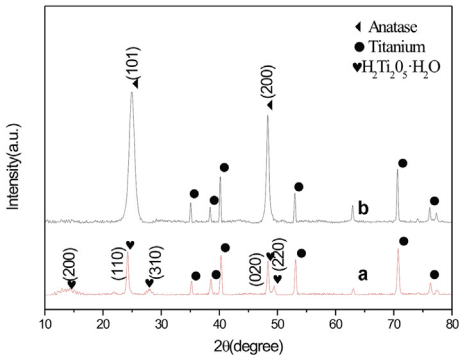

Fig. 1. X-ray diffraction patterns of $H_2Ti_2O_5 \cdot H_2O$ nanowire film on titanium foil prepared by hydrothermal growth in 1 M NaOH aqueous solution at 220 °C for 24 h and then by ion exchanged (a), and further annealed at 450 °C for 30 min (b).

Zview software. Photovoltaic tests were carried out by measuring the Current–Voltage (I–V) characteristic curves under simulated AM 1.5 G solar illumination at 100 mW cm^{-2} with #94043A solar simulator (PVIV-94043A, Newport, USA); and incident-photo-to-current conversion efficiency (IPCE) curves were measured as a function of wavelength from 300 nm to 800 nm using the Newport IPCE system (Newport, USA). All of the samples were measured five times and the average data were taken. The active area of DSCs was 0.12 cm^2 (0.3 × 0.4 cm^2).

3. Results and discussion

Fig. 1 shows the X-ray diffraction patterns of the synthesized sample on titanium foil by ion exchanged (a), and further annealed at 450 °C (b). Except the characteristic peaks corresponding to the titanium foil, all of the other peaks in Fig. 1(a) can be readily indexed to $H_2Ti_2O_5 \cdot H_2O$ according to the JCPDS#47-0124, and the appeared peaks in Fig. 1(b) can be indexed as the anatase TiO_2 according to the JCPDS#21-1272. Moreover, no characteristic peaks of other impurities are observed, which indicates that the product has high purity and the $H_2Ti_2O_5 \cdot H_2O$ can totally be converted to anatase TiO_2 with a high temperature sintering process.

The typical cross-sectional FESEM images of TiO_2 nanowire arrays are shown in Fig. 2. All of the as-grown TiO_2 nanowires are nearly perpendicular to the substrates. The thickness of the TiO_2 nanowire arrays increases gradually with prolonging hydrothermal duration, and then decreases. The thickest one can attain to 15.9 μm with 24 h hydrothermal duration. The average diameter of these TiO_2 nanowires is about 70–80 nm, and some bigger ones also appear in the samples with longer hydrothermal duration as shown in the enlarged images in Fig. 2.

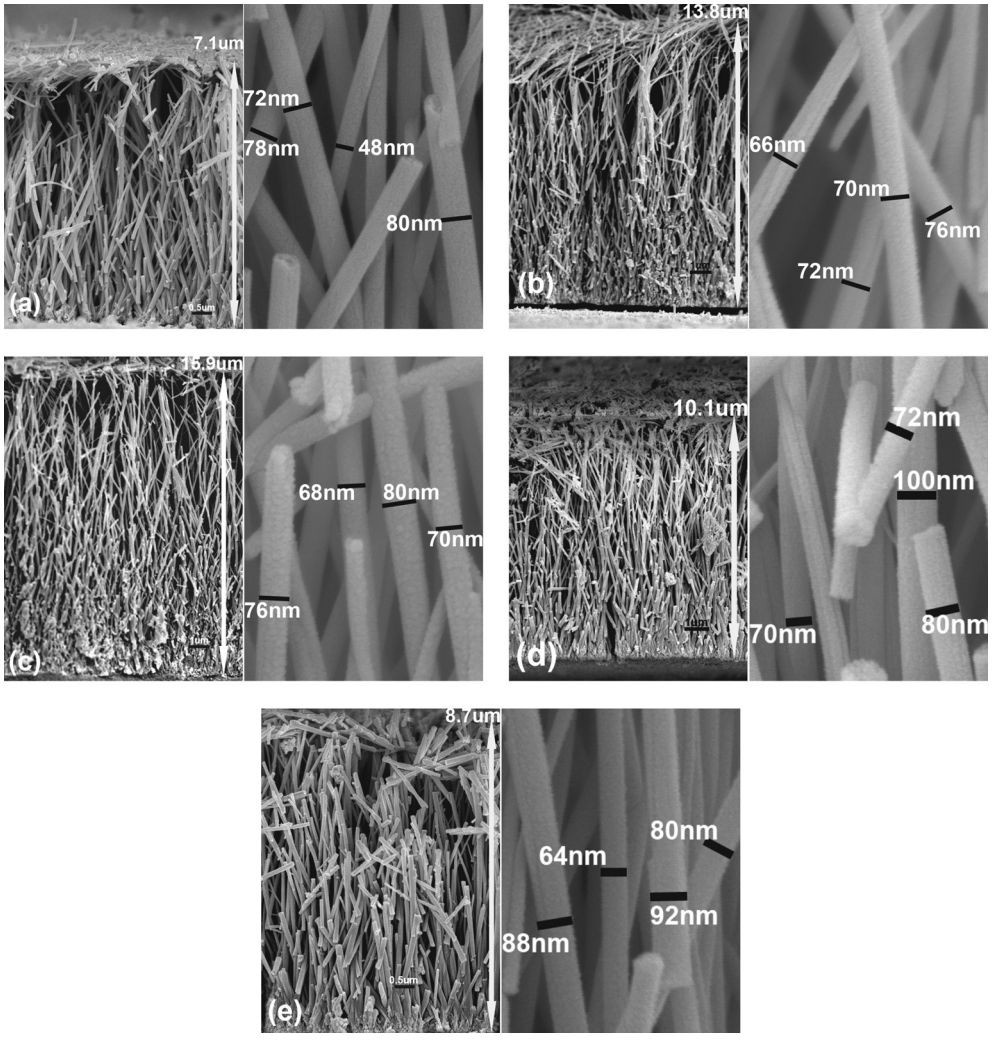

Fig. 2. Cross-sectional FESEM images of TiO_2 nanowire arrays with different hydrothermal duration. (a) 16 h, (b) 20 h, (c) 24 h, (d) 28 h, (e) 32 h.

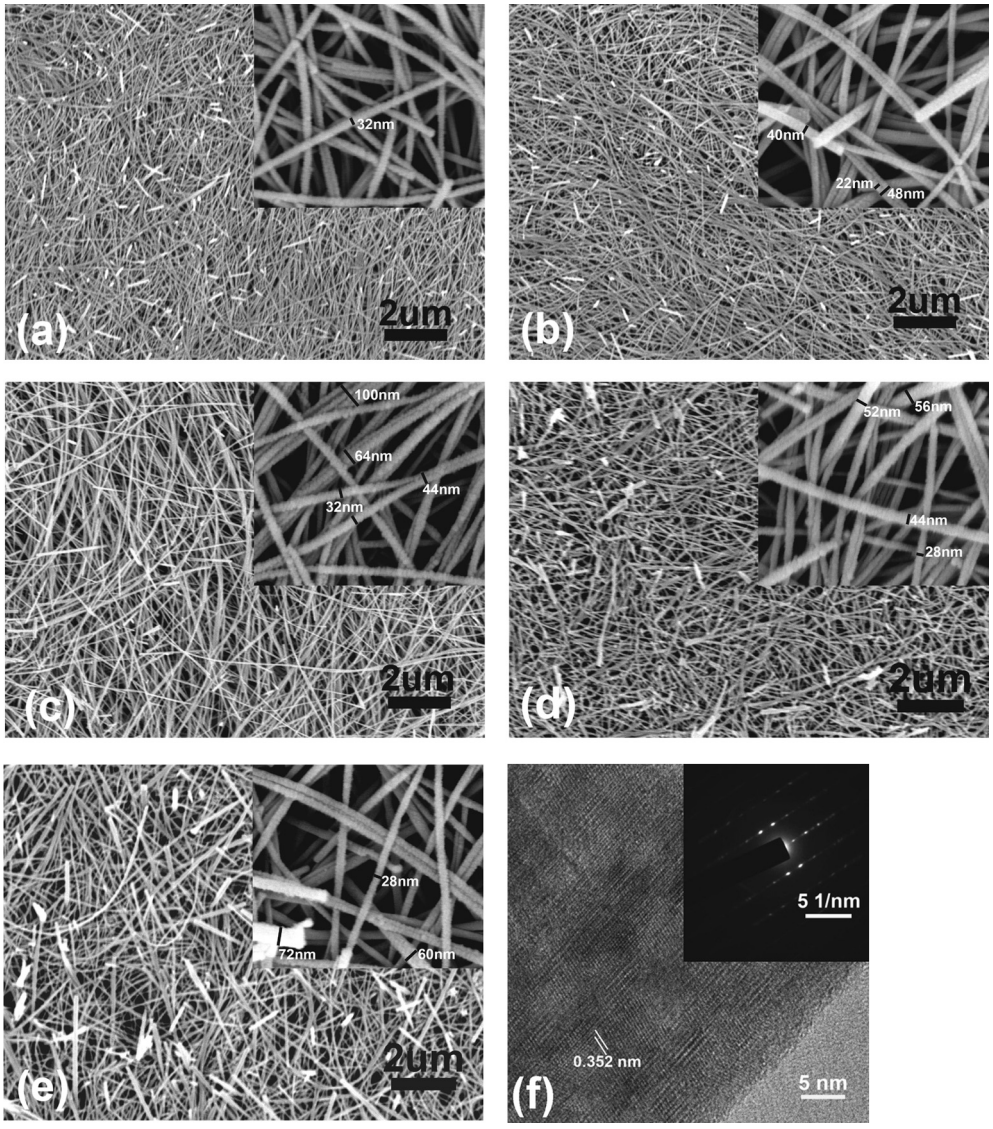

Fig. 3. Top view FESEM images of TiO_2 nanowire arrays with different hydrothermal duration. (a) 16 h, (b) 20 h, (c) 24 h, (d) 28 h, (e) 32 h; (f) HRTEM image and SAED patterns of TiO_2 nanowires.

The top view FESEM images of TiO_2 nanowire arrays are shown in Fig. 3. Owing to the large ratio of length to diameter, the TiO_2 nanowires on the surface of arrays can form a loose and porous 3D nano-network, which are very similar to electrospun nanofibers [18]. The enlarged images in Fig. 3 show that the diameter of these TiO_2 nanowires is about 30–40 nm. Some bigger ones are formed by prolonging hydrothermal duration, at the same time, parts of TiO_2 nanowires tend to aggregate in parallel to form nanowire

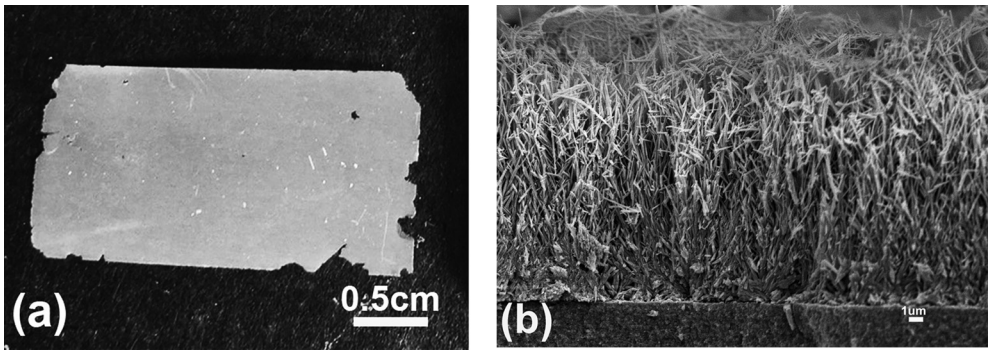

Fig. 4. Digital photo of a large area free-standing TiO_2 nanowire membrane (a), and cross-sectional SEM image of the membrane cohered on an FTO glass with the TiO_2 nanoparticle cementing agent.

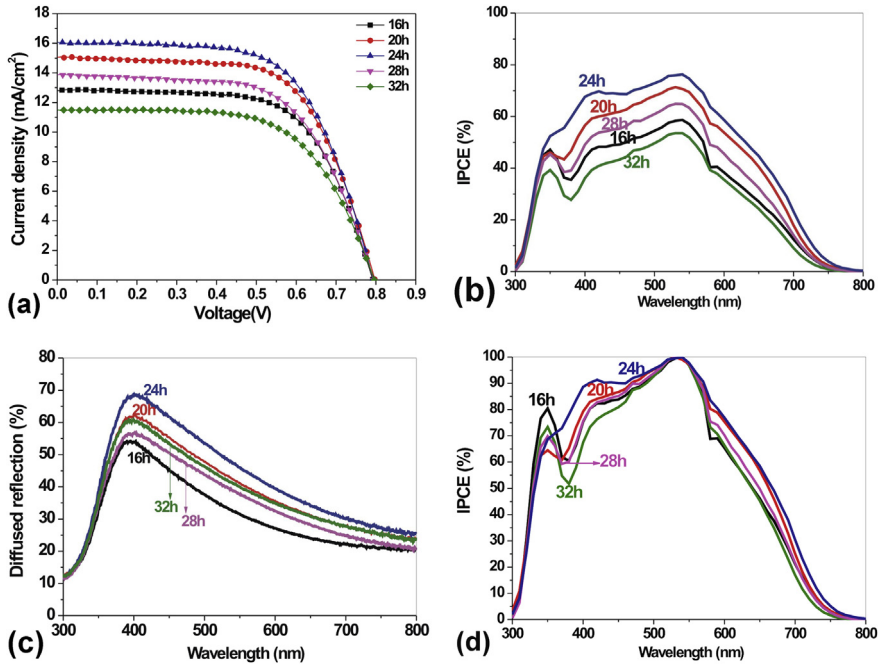

Fig. 5. *I–V* (a) and IPCE (b) curves of the DSCs containing TiO_2 nanowire membranes prepared with different hydrothermal duration, diffused reflection spectra of the photoanodes without adsorbing dyes (c), and the normalized IPCE spectra (d).

bundles. The changed morphologies of the samples with different hydrothermal duration give us information that the extra long hydrothermal duration may result in thinner TiO_2 nanowire arrays with some aggregated nanowire bundles on the surface, which may be owing to the dissolution and re-growth of some parts of the TiO_2 nanowires [14]. Furthermore, the high-resolution transmission electron microscope (HRTEM) image and the selected area electron diffraction (SAED) pattern shown in Fig. 3(f) confirm that the ultra-long TiO_2 nanowire is single crystalline.

TiO_2 nanowire membranes on the Ti foils can be used to fabricate back-side illuminated photoanodes. In this way, the photons should irradiate from the counter electrode and pass through electrolyte layer, resulting in attenuated light intensity. Another way is to peel of the TiO_2 nanowire membranes and bond them on FTO glasses to fabricate front-side illuminated photoanodes. So the photons can directly illuminate on the photoanodes. The free-standing TiO_2 nanowire membranes can be easily separated from Ti foils with anodization and chemical etching method and cohered on FTO glasses using a paste containing TiO_2 nanocrystalline particles with size about 10–20 nm [15,16,19]. Fig. 4 shows a digital photo of the large area free-standing TiO_2 nanowire membrane and the cross-sectional SEM image of the membrane bonded with TiO_2 nanocrystalline particles. It is seen that a crack-free TiO_2 nanowire membrane has been successfully peeled from the Ti foil and it can be well cemented by the TiO_2 nanocrystalline particles.

Table 1
Photovoltaic parameters of the DSCs shown in Fig. 5.

DSCs	V_{oc} (V)	J_{sc} (mA cm^{-2})	FF	Eff (%)	Adsorb dye (mol cm^{-2})
16 h	0.792 ± 0.005	12.88 ± 0.12	0.644 ± 0.007	6.57 ± 0.18	0.684×10^{-7}
20 h	0.797 ± 0.004	15.13 ± 0.09	0.637 ± 0.011	7.68 ± 0.22	0.880×10^{-7}
24 h	0.793 ± 0.009	16.08 ± 0.08	0.631 ± 0.009	8.05 ± 0.24	0.960×10^{-7}
28 h	0.794 ± 0.003	13.92 ± 0.05	0.618 ± 0.012	6.83 ± 0.18	0.664×10^{-7}
32 h	0.796 ± 0.001	11.52 ± 0.07	0.625 ± 0.007	5.73 ± 0.11	0.556×10^{-7}

Photovoltaic performance of the DSCs containing TiO_2 nanowire membranes prepared with different hydrothermal duration (according to the hydrothermal duration, the related DSCs are named as DSC-16, DSC-20, DSC-24, DSC-28, and DSC-32, respectively) is shown in Fig. 5. The related parameters such as open-circuit voltage (V_{oc}), short-circuit current density (J_{sc}), fill factor (FF), and power conversion efficiency (Eff) are summarized in Table 1. From Fig. 5(a) and Table 1, the highest value of Eff about 8.05% can be obtained in the DSC-24. Either shortening or prolonging hydrothermal duration in preparing TiO_2 nanowire membranes results in poorer photovoltaic performance of the DSCs. We can see that the different photovoltaic performance of the DSCs is mainly originated from the variation of J_{sc}. In the DSC-24, the values of J_{sc} and IPCE are about 16.08 mA cm^{-2} and 76.31%, respectively, higher than the other DSCs. The change tendency of IPCE data shown in Fig. 5(b) is in keeping with that of the values of J_{sc}. Reproducibility of DSC with best performance (DSC-24) is evaluated by preparing the other 8 samples of DSC-24 and measuring their photovoltaic performance. The data listed in Table 2 validate the stable performance of DSC-24s.

Dye-loading amounts of the photoanodes based on TiO_2 nanowire membranes prepared with different hydrothermal duration are estimated by measuring the absorption of dye solution desorbed from the photoanodes with 1 mM NaOH ethanol solution and

Table 2
Reproducibility of photovoltaic performance of DSC-24s.

DSC-24	V_{oc} (V)	J_{sc} (mA cm^{-2})	FF	Eff (%)
0	0.793	16.08	0.631	8.05
1	0.801	15.24	0.650	7.93
2	0.794	16.29	0.618	7.99
3	0.801	16.88	0.594	8.03
4	0.811	16.36	0.603	8.00
5	0.801	16.40	0.630	8.28
6	0.797	15.55	0.637	7.89
7	0.788	16.45	0.618	8.01
8	0.799	16.60	0.607	8.05

listed in Table 1. From the data, it is seen that dye-loading amounts of the photoanodes are increased gradually and then decreased by prolonging hydrothermal duration; the highest value is obtained from the photoanode containing TiO_2 nanowire membrane prepared with 24 h hydrothermal duration.

As aforementioned, after 24 h hydrothermal duration, the TiO_2 nanowires can form the thickest membrane about 15.9 μm. On top of the membrane, the TiO_2 nanowires are uniform and slender. Although some nanowire bundles are formed, they are generally composed with these slender TiO_2 nanowires with diameter about 32 nm. The thickness of other TiO_2 nanowire membranes prepared with shorter or longer hydrothermal duration is thinner. And the TiO_2 nanowires on top of these samples are non-uniform. The changed thickness of the membranes and the different morphologies of the TiO_2 nanowires on top of the membranes influence the internal surface area of the membranes for dye-loading, finally resulting in different dye-loading amounts. Furthermore, they also influence light scattering ability of the membranes. As shown in Fig. 5(c), the change tendency of light scattering ability of these membranes is nearly consistent with the thickness of the membranes except for the one prepared with 32 h hydrothermal duration. The strong light scattering ability of the sample with 32 h hydrothermal duration is mainly due to its special structure of composing some shorter and fractured TiO_2 nanowires.

The changed dye-loading and light scattering abilities of the photoanodes influence light harvest efficiencies, which further affect the values of J_{sc}. For better understanding the roles of enhanced dye-loading amounts and light scattering ability on the improved values of J_{sc}, each IPCE maximum [Fig. 5(b)] is normalized to 100% and shown in Fig. 5(d). In the short-wavelength region (300–550 nm), the improvement can be attributed primarily to the enhanced dye-loading amounts. The evidence is that although light scattering ability of the photoanode in DSC-28 is higher than that of the photoanode in DSC-16 (the two photoanodes show similar dye-loading amounts as listed in Table 1), it does not produce higher IPCE values in 300–550 nm wavelengths in DSC-28 than that of DSC-16. Whilst, in the long-wavelength region (550–750 nm) where the N719 dye has low absorption for incident light, the improved IPCE values mainly originate from the enhanced light scattering ability of the photoanodes. We can see that the variation trend of IPCE values of these DSCs in 550–750 nm wavelengths is mostly accordance with that of light scattering ability of the photoanodes in the cells except for DSC-32. In DSC-32, the high light scattering ability does not lead to high IPCE values in 550–750 nm wavelengths. The reason may be owing to its poor electron transport property as discussed below.

Charge transfer dynamics in the DSCs are investigated with intensity modulated photocurrent spectroscopy (IMPS) and intensity

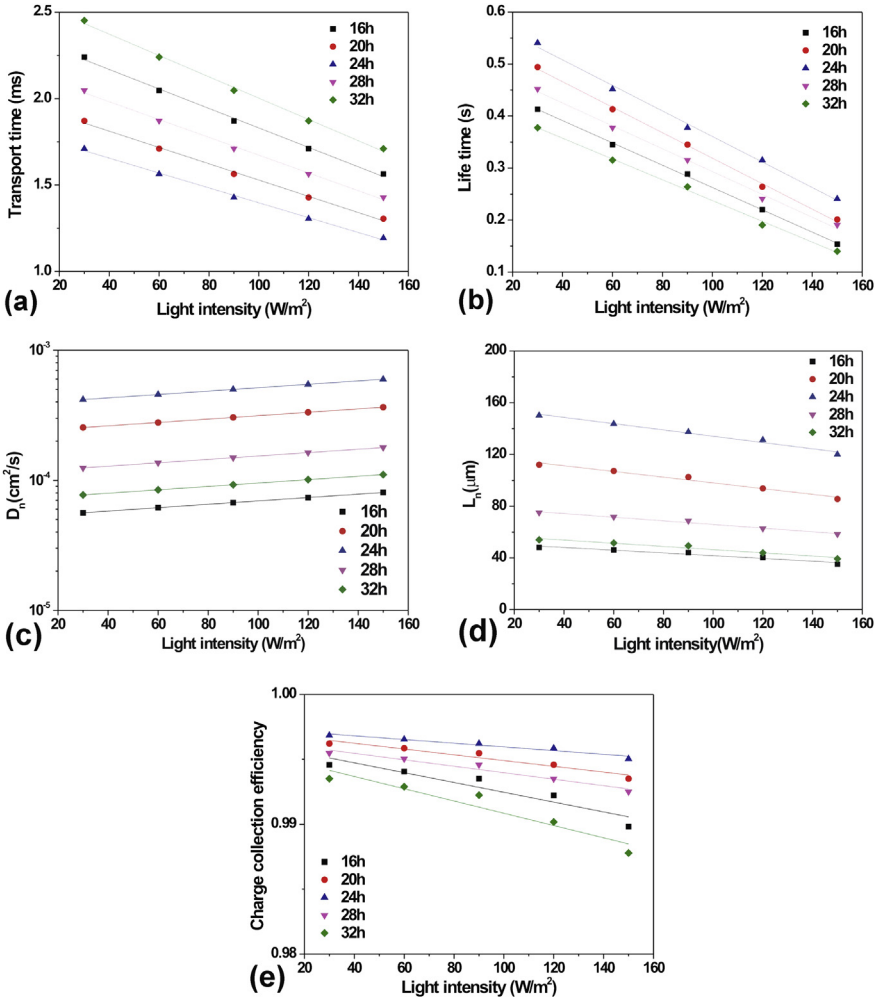

Fig. 6. Light intensity dependence of the charge transport time (a), the life time (b), the electron diffusion coefficient (D_n) (c), the effective electron diffusion length (L_n) (d), and the charge collection efficiency (e) of the DSCs.

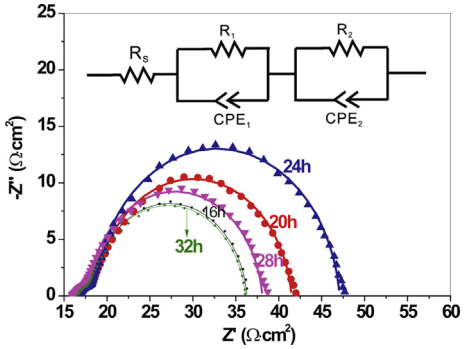

Fig. 7. Electrochemical impedance spectra of DSCs based on TiO_2 nanowire membranes prepared with different hydrothermal duration. The inset is the equivalent circuit applied to fit the data.

modulated photovoltage spectroscopy (IMVS). The charge transport time and life time can be obtained using the expressions of τ_d (transport time) $= (2\pi f_d)^{-1}$ and τ_r (recombination life time) $= (2\pi f_r)^{-1}$, where f_d and f_r are the characteristic frequency minimums of the IMPS and IMVS imaginary components, respectively [20]. Furthermore, the electron diffusion coefficient (D_n), the effective electron diffusion length (L_n), and the charge collection efficiency (η_{cc}) also can be calculated with the data of τ_d and τ_r according to the equations of $D_n = d^2/(4\tau_d)$, $L_n = (D_n \times \tau_r)^{0.5}$, and $\eta_{cc} = 1 - \tau_d/\tau_r$, where d is film thickness [21,22].

Light intensity dependence of the values of τ_d, τ_r, D_n, L_n, and η_{cc} of the DSCs are shown in Fig. 6. From Fig. 6(a) and (b), one can observe that the value of τ_d decreases gradually by prolonging hydrothermal duration to 24 h, and then increases; whilst the value of τ_r presents a reversal change tendency compared with that of τ_d. The shorter τ_d means the faster electron transport rate; and the longer τ_r represents the slower charge recombination in the DSC [23]. So the DSC-24 shows perfect charge transport dynamic versus the other samples. The values of D_n and L_n shown in Fig. 6(c) and (d) further confirm the excellent charge transport properties in the DSC-24.

Electrochemical impedance spectroscopy (EIS) is also tested for better understanding charge transfer and recombination dynamics within DSCs. Fig. 7 shows typical Nyquist plots of the DSCs. The important EIS parameters can be fitted with the equal circuit inside the figure. The key resistance element of R_2 calculated from the large semicircle in low-frequency region is related to the recombination resistance at the interface of TiO_2/dye/electrolyte [24]. As shown in Table 2, the R_2 values of the DSCs increase to the highest value by prolonging hydrothermal duration to 24 h, and then decrease with longer hydrothermal duration, indicating a slower recombination rate occurred within DSC-24 than other samples. The τ_r values can also be calculated with the equation of $\tau_r = R_2 \times CPE_2$. The variation of τ_r values listed in Table 2 is consistent with that of the values obtained from IMVS. Table 3

From FESEM images shown in Figs. 2 and 3, it is found that by going along with prolonging hydrothermal duration to 24 h, the TiO_2 nanowire membrane can form ideal structure with homogeneously slender TiO_2 nanowires on the top of the film and the thickest thickness compared with the other samples. The insufficient or excess hydrothermal duration results in forming thinner films and some shorter and fractured TiO_2 nanowires on the top of the films. The structural difference may response for the different charge transport dynamics of these TiO_2 nanowire membranes in the DSCs. Fig. 6(e) reveals that the DSCs with these TiO_2 nanowire membranes all have high charge collection efficiency above 98%, and the DSC-24 has the highest value. So the excellent charge transport property in the DSC-24 also contributes better photovoltaic performance.

Table 3
Simulated values of recombination resistance (R_2) and electron life time (τ_r) shown in Fig. 7.

DSCs	R_2 (Ω cm^2)	τ_r (S)
16 h	17.92	0.125
20 h	22.55	0.169
24 h	28.41	0.232
28 h	20.01	0.138
32 h	17.74	0.119

4. Conclusions

In conclusion, high-efficiency dye-sensitized solar cells (DSCs) based on 3D networks of ultra-long single crystalline TiO_2 nanowires are fabricated. By hydrothermal reaction of Ti foils in alkali aqueous solution, following ion exchange and high temperature sintering processes, the ultra-long single crystalline TiO_2 nanowires can be prepared. Due to the long enough of TiO_2 nanowires, they not only form 1D arrays perpendicular to Ti foils, but also extend to form 3D network structure on the top-side of the arrays. The special structure of the TiO_2 nanowire membranes can be easily peeled from Ti foils to fabricate front-side illuminated photoanodes. It is found that through changing the hydrothermal duration, the TiO_2 nanowire membrane based photoanodes show changed dye-loading amounts, light scattering ability, and charge transport dynamics. The optimized hydrothermal duration about 24 h can be found. The DSC with TiO_2 nanowire membrane prepared by 24 h hydrothermal duration present the highest power conversion efficiency about 8.05%, originating from its best dye-loading and light scattering abilities and excellent charge transport properties.

Acknowledgments

The authors gratefully acknowledge the financial supports by the National Natural Science Foundation of China (Nos. U1205112 and 51002053); the Key Project of the Chinese Ministry of Education (212206); the Programs for Prominent Young Talents and New Century Excellent Talents in Fujian Province University; the Promotion Program for Yong and Middle-aged Teacher in Science and Technology Research of Huaqiao University (ZQN-YX102).

References

[1] A. Yella, H.W. Lee, H.N. Tsao, C. Yi, A.K. Chandiran, M.K. Nazeeruddin, E.W.G. Diau, C.Y. Yeh, S.M. Zakeeruddin, M. Grätzel, Science 334 (2011) 629.
[2] Z.S. Wang, H. Kawauchi, T. Kashima, H. Arakawa, Coord. Chem. Rev. 248 (2004) 1381.
[3] B. O'Regan, M. Grätzel, Nature 353 (1991) 737.
[4] J. Nelson, Phys. Rev. B 59 (1999) 15374.
[5] J.V. Lagemaat, A.J. Frank, J. Phys. Chem. B 105 (2001) 11194.
[6] K.D. Benkstein, N. Kopidakis, J.V. Lagemaat, A.J. Frank, J. Phys. Chem. B 107 (2003) 7759–7767.
[7] M. Law, L. Greene, J.C. Johnson, R. Saykally, P. Yang, Nat. Mater. 4 (2005) 455.
[8] J.R. Jennings, A. Ghicov, L.M. Peter, P. Schmuki, A.B. Walker, J. Am. Chem. Soc. 130 (2008) 13364.
[9] M. Lv, D. Zheng, M. Ye, J. Xiao, W. Guo, Y. Lai, L. Sun, Energy Environ. Sci. 6 (2013) 1615.
[10] W.Q. Wu, B.X. Lei, H.S. Rao, Y.F. Xu, Y.F. Wang, C.Y. Su, D.B. Kuang, Sci. Rep. http://dx.doi.org/10.1038/srep01352.
[11] J.Y. Liao, B.X. Lei, H.Y. Chen, D.B. Kuang, C.Y. Su, Energy Environ. Sci. 5 (2012) 5750.
[12] C. Xu, J. Wu, U.V. Desai, D. Gao, J. Am. Chem. Soc. 133 (2011) 8122.
[13] W.Q. Wu, Y.F. Xu, C.Y. Su, D.B. Kuang, Energy Environ. Sci. 7 (2014) 644.
[14] X. Peng, A. Chen, Adv. Funct. Mater. 16 (2006) 1355.
[15] J. Choi, S.H. Park, Y.S. Kwon, J. Lim, I.Y. Song, T. Park, Chem. Comm. 48 (2012) 8748.

[16] S.W. Gao, Z. Lan, W.X. Wu, L.F. Que, J.H. Wu, J.M. Lin, M.L. Huang, Acta Phys. Chim. Sin. 30 (2014) 446.
[17] L.F. Que, Z. Lan, W.X. Wu, J.H. Wu, J.M. Lin, M.L. Huang, J. Power Sources (2014) under review.
[18] Q. Mu, Y. Li, H. Wang, Q. Zhang, CrystEngComm 13 (2011) 6258.
[19] Q. Chen, D. Xu, J. Phys. Chem. C 113 (2009) 6310.
[20] H.X. Wang, P.G. Nicholson, L. Peter, S.M. Zakeeruddin, M. Gratzel, J. Phys. Chem. C 114 (2010) 14300.
[21] S.M. Wang, W.W. Dong, R.H. Tao, Z.H. Deng, J.Z. Shao, L.H. Hu, J. Zhu, X.D. Fang, J. Power Sources 235 (2013) 193.
[22] W.Q. Wu, H.S. Rao, H.L. Feng, X.D. Guo, C.Y. Su, D.B. Kuang, J. Power Sources 260 (2014) 6.
[23] K. Zhu, T.B. Vinzant, N.R. Neale, A.J. Frank, Nano Lett. 7 (2007) 3739.
[24] F. Fabregat-Santiago, J. Bisquert, E. Palomares, L. Otero, D.B. Kuang, S.M. Zakeeruddin, M. Grätzel, J. Phys. Chem. C 111 (2007) 6550.